T_{RM} integrins CD103 and CD49a differentially support adherence and motility after resolution of influenza virus infection

Emma C. Reilly[a], Kris Lambert Emo[a], Patrick M. Buckley[a], Nicholas S. Reilly[b], Ian Smith[a], Francisco A. Chaves[a], Hongmei Yang[c], Patrick W. Oakes[b,d], and David J. Topham[a,e,1]

[a]Center for Vaccine Biology and Immunology, University of Rochester Medical Center, Rochester, NY 14642; [b]Department of Physics and Astronomy, University of Rochester Medical Center, Rochester, NY 14642; [c]Department of Biostatistics and Computational Biology, University of Rochester Medical Center, Rochester, NY 14642; [d]Department of Biology, University of Rochester Medical Center, Rochester, NY 14642; and [e]Department of Microbiology and Immunology, University of Rochester Medical Center, Rochester, NY 14642

Edited by Akiko Iwasaki, Yale University, New Haven, CT, and approved April 17, 2020 (received for review September 10, 2019)

Tissue-resident memory CD8 T (T_{RM}) cells are a unique immune memory subset that develops and remains in peripheral tissues at the site of infection, providing future host resistance upon reexposure to that pathogen. In the pulmonary system, T_{RM} are identified through S1P antagonist CD69 and expression of integrins CD103/β7 and CD49a/CD29(β1). Contrary to the established role of CD69 on CD8 T cells, the functions of CD103 and CD49a on this population are not well defined. This study examines the expression patterns and functions of CD103 and CD49a with a specific focus on their impact on T cell motility during influenza virus infection. We show that the T_{RM} cell surface phenotype develops by 2 wk postinfection, with the majority of the population expressing CD49a and a subset that is also positive for CD103. Despite a previously established role in retaining T_{RM} in peripheral tissues, CD49a facilitates locomotion of virus-specific CD8 T cells, both in vitro and in vivo. These results demonstrate that CD49a may contribute to local surveillance mechanisms of the T_{RM} population.

influenza | T cell | integrin | memory

Tissue-resident memory CD8 T cells (T_{RM}) are a critical and unique component of the adaptive immune system (1–3). Unlike circulating memory cell populations (T_{CM} and T_{EM}), they reside within peripheral tissues after clearance of a pathogen or immunological insult and dictate downstream innate and adaptive responses upon reactivation (2, 4). In the absence of T_{RM} cells, hosts display increased susceptibility and illness severity when exposed to related pathogens (2). Current vaccination strategies, especially for influenza, focus on generating protective antibodies, and these approaches do not elicit effective CD8 T cell–mediated protection. Neutralizing antibodies classically bind external epitopes of pathogens and, on the influenza virion, target the head region of the rapidly evolving hemagglutinin proteins (5–7). In contrast, T_{RM} cells primarily respond to internally derived pathogen epitopes which are less prone to external pressures and mutation (8). The capability to induce localized memory T cells through vaccination will facilitate increased cross protection against a greater breadth of influenza strains. However, we need to better understand many aspects of T_{RM} biology in order to optimize their generation and maintenance.

Parabiosis experiments established that the T_{RM} are a noncirculating subset (9, 10), and specific surface markers have been identified to minimize the need for this procedure. T_{RM} populations display phenotypic variation between tissue types; however, the majority express CD69 and integrins CD49a/CD29 and CD103/β7 to some degree (11, 12). Early studies suggested that CD69 was essential for the T_{RM} population in the skin and lung (13, 14); however, its contribution to T_{RM} maintenance was recently shown to function primarily in the kidneys, with less of a requirement in other peripheral sites (10, 15). In the lung, CD49a is necessary for the survival of T_{RM} cells, in part through engagement of its ligand collagen IV, which limits apoptosis (2, 16). Absence of CD49a results in increased susceptibility to a lethal challenge with a heterosubtypic influenza A virus, resulting from a more rapid decline in T_{RM} cell numbers. In other sites, lack of CD49a impacts the accumulation of gut-resident intraepithelial CD8 T cells (17), and blocking CD49a augments T cell positioning and the subsequent immune response in a xenotransplant model of psoriasis (18). Eliminating the E-cadherin binding CD103 also results in a diminished population of T_{RM} cells in some tissues (13, 19–21). However, the CD103 requirement is less clear, and its functions in vivo may support initial accumulation of the cells rather than long-term persistence (21, 22).

In other cell types, integrins facilitate attachment and interactions with other cell populations and support motility (23, 24). Early studies provide some insight into the contributions of CD49a and CD103 to the preservation of the T_{RM} population through blocking or deletion of the integrins (2, 19, 20, 21).These experiments establish a role for these integrins as markers

Significance

Current influenza vaccination strategies require annual immunizations, with fairly low efficacy rates. One technique to improve protection against a greater breadth of influenza viruses is to elicit broadly cross-reactive cell-mediated immunity and generate a local population of cytotoxic T cells to respond to conserved regions of circulating viruses. However, this approach requires improved understanding of how these cells migrate within and attach to the tissue in order to persist and offer long-term immunity. This study investigates how receptors on the T cell surface impact the cell's ability to interact with the tissue and provide evidence of which of these receptors are essential for protection. Furthermore, these studies reveal functional in vivo mechanisms of cellular markers used to characterize T_{RM}.

Author contributions: E.C.R., K.L.E., N.S.R., F.A.C., P.W.O., and D.J.T. designed research; E.C.R., K.L.E., P.M.B., N.S.R., F.A.C., and P.W.O. performed research; I.S. and F.A.C. contributed new reagents/analytic tools; E.C.R., K.L.E., P.M.B., N.S.R., I.S., H.Y., P.W.O., and D.J.T. analyzed data; E.C.R. and D.J.T. wrote the paper; and I.S. contributed new analytical code.

The authors declare no competing interest.

This article is a PNAS Direct Submission.

Data deposition: The data sets in this paper are available in the NIH public immunology data repository ImmPort (https://www.immport.org) under accession number SDY1631.

[1]To whom correspondence may be addressed. Email: david_topham@urmc.rochester.edu.

This article contains supporting information online at https://www.pnas.org/lookup/suppl/doi:10.1073/pnas.1915681117/-/DCSupplemental.

First published May 21, 2020.

essential for optimal T_{RM} maintenance but do not delve into the direct interactions that lead to these functional ramifications. Therefore, we investigated how these integrins regulate interactions with the tissue through adherence and motility with the ultimate aim of determining whether these integrins equally contribute to host protection.

Results

Pulmonary CD8 T Cells Express CD49a and CD103 Early after Influenza Virus Clearance. T_{RM} cells are classically identified through expression of CD69 and integrins CD103 and CD49a. CD69 limits egress of T_{RM} cells from tissues by acting as an antagonist to S1P and reduces responsiveness to S1P1 gradients that direct the cells toward the draining lymphatics (25, 26). The functions of the surface integrins CD103 and CD49a on T cells are less well appreciated. Additionally, the temporal development of this surface phenotype is not well characterized. Bona fide T_{RM} cells can be found in the airways, lung tissue, and trachea at 3 mo postinfection (2), and these cells express CD49a and/or CD103. We asked whether this phenotype arose early after virus clearance by comparing the integrin phenotypes at 2 wk postinfection, with T_{RM} cells present at 3 mo. CD8 T cells were examined in two different models of influenza virus infection. In the first, C57BL/6 mice were infected intranasally with H3N2 influenza A virus HKx31. In the second model, which is used for all imaging-based experiments described in this study, GFP OT-I cells were adoptively transferred prior to infection with an HKx31 variant expressing the OvaI SIINFEKL peptide in the neuraminidase stalk (27). To clearly separate cells in the tissue from cells circulating or intimately associated with the vasculature, antibody was introduced intravascularly prior to harvesting cells from the airways, tracheal tissue, or lung tissue (28, 29). Close to 100% of virus-specific CD8 T cells in the airways were negative for intravascular labeling, indicating that almost all of the cells are within the tissue parenchyma (*SI Appendix*, Figs. S1 and S2). At 3 mo after HKx31 infection, greater than 80% of NP/PA tetramer positive T cells in the airways express CD49a, with ∼15% coexpressing both integrins (Fig. 1*A*). This phenotype was comparable in the transfer system where airway OT-I cells were examined (Fig. 1*A*). Only 10 to 50% of CD8 T cells in the lung were protected from intravenous (IV) labeling, depending on the time point evaluated (*SI Appendix*, Fig. S2). For this reason, both the tissue and vasculature associated populations were examined within this organ. Approximately 35% of CD8 T cells within the tissue express only CD49a, with 5 to 30% expressing both integrins (Fig. 1*B*). A subset of vascular CD8 T cells express CD49a alone, and only a small subset coexpresses CD103 (Fig. 1*B*). Of note, within the CD49a positive subsets, tissue CD8 T cells have significantly higher levels of CD49a staining (*SI Appendix*, Fig. S3). Unexpectedly, cells in the trachea were almost exclusively IV protected, and virus-specific CD8 T cells at 3 mo postinfection were predominantly CD49a/CD103 double positive in both systems (*SI Appendix*, Fig. S2 and Fig. 1*C*).

Cells examined in wild-type mice at day 14 postinfection demonstrated over 80% positivity for CD49a with a frequency of over 35% expressing CD103, and this phenotype was consistent with the OT-I transfer system (Fig. 1*A*). Trachea and lung OT-I T cells within the tissue looked remarkably similar at this time point, with over 70% expressing CD49a and roughly one-half of those cells also expressing CD103 (Fig. 1 *B* and *C*). Comparable to the T_{RM} time point, a subset of vascular labeled CD8 T cells in the lungs expressed CD49a alone; however, again, the level of expression was significantly reduced compared with cells from the tissue proper (*SI Appendix*, Fig. S3). The high proportions and comparable integrin expression signatures at these time points suggest they are generated early after viral clearance, consistent with the postulation that T_{RM} develop during resolution and repair of the damaged airways.

CD49a and CD103 Differentially Affect T Cell Behavior In Vitro. CD49a and CD103 have been shown to bind and interact with collagen and E-cadherin, respectively (30–34). However, in T cells, the understanding of how these interactions regulate motility is not fully established. Using a two-dimensional (2D) in vitro system, we first asked the question, Do CD49a and CD103 facilitate migration? On day 14 postinfection, virus-specific CD8 T cells identified through expression of GFP were imaged on mouse collagen IV (four) or E-cadherin. GFP OT-I T cells on collagen IV displayed robust motility, with median speeds of 4.48 μm/min (interquartile range [IQR] of 3.85), displacement rates of 0.79 μm/min (IQR of 2.29), and directionality as measured by straightness of 0.20 (IQR of 0.33) (Fig. 2 *A*–*D*). The addition of CD49a blocking antibody resulted in reduced speeds, displacement, and straightness, suggesting that the migration was mediated through the CD49a–collagen IV interaction (Fig. 2 *A*–*E* and Movie S1). To verify that the observed effect was not indicative of a deterioration of the health of the cells, an antibody against CD103 was added to cells migrating

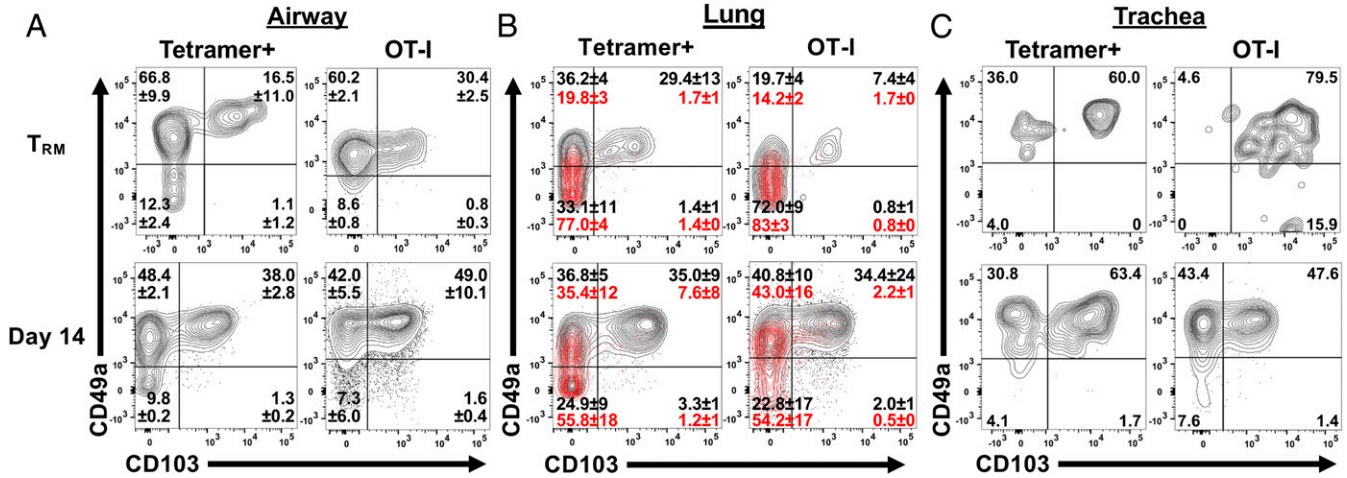

Fig. 1. T_{RM} integrin phenotype arises by 2 wk postinfection. Mice were infected with HKx31 influenza virus, or OT-I CD8 T cells were adoptively transferred prior to infection with HKx31-Ova (OT-I). Tissue virus-specific cells (black) or vasculature-associated cells (red) were assessed by a combination of NP and PA tetramer (Tetramer+) or by gating on OT-I CD8 T cells (OT-I) at 3 mo or 14 d postinfection. Cells were examined in the airways through bronchoalveolar lavage (*A*), lung tissue (*B*), and trachea (*C*). Results shown are mean ± SD from one representative of three independent experiments.

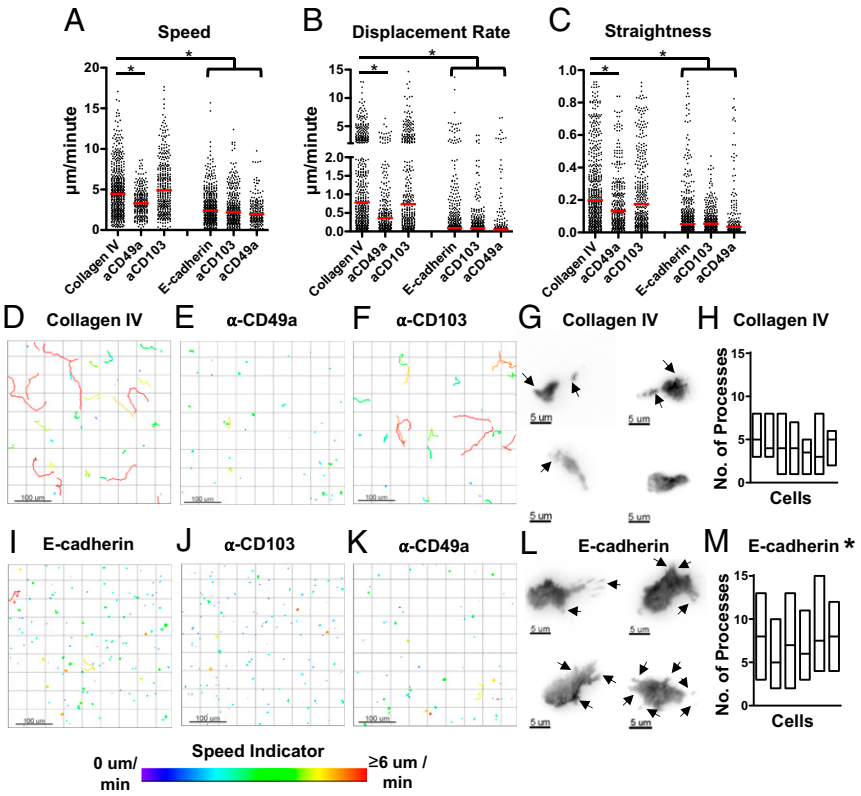

Fig. 2. CD49a and CD103 differentially affect T cell behavior in vitro. OT-I T cells were extracted and negatively enriched from influenza-infected lung at day 14 postinfection. Cell motility was quantified on mouse collagen IV or E-cadherin before and after addition of blocking antibody. Speed (track length/time) (*A*), displacement rate (displacement/time) (*B*), and straightness (total track length/displacement) (*C*) were calculated. Representative tracks from one experiment are shown, with color indicating average track speed (*D–F* and *I–K*). Each wild-type condition includes data from six independent experiments and each treatment condition includes data from three independent experiments. Representative TIRF images on collagen and E-cadherin with arrows showing examples of cellular processes (*G* and *L*). Number of processes, shown as median with range for six individual cells on each surface (*H* and *M*). Data in *A–C* are from six control mice and three for each experimental condition. The red bar indicates the median. Significance was first established within each independent experiment and also with compiled data. $*P < 0.05$.

on collagen. Blocking CD103 on collagen had no effect on motility, establishing that cells were migrating on collagen IV in a CD49a-dependent manner (Fig. 2 *A–C* and *F*). Cells plated on E-cadherin showed minimal displacement compared with cells on collagen IV (Fig. 2 *A–C* and *I*). The majority of cells remained fixed at a single point, and the addition of a CD103 blocking antibody did not show any overall changes in speed, displacement, or straightness (Fig. 2 *A–C*, *I*, and *J* and Movie S2). Blocking CD49a on E-cadherin also did not have any effect, compared with control cells (Fig. 2 *A–C*, *I*, and *K*). To more closely examine these integrins engaging their respective substrates, cells were imaged on collagen IV and E-cadherin using total internal reflection fluorescence (TIRF) microscopy. Cells on the collagen IV surface appeared elongated and, even in the presence of tail-like structures, continued to migrate (Fig. 2*G* and Movie S3). Cells on collagen had a median of 4 (IQR of 2) cellular processes per cell observed by TIRF microscopy (Fig. 2 *G* and *H* and *SI Appendix*, Fig. S4). In stark contrast, cells on E-cadherin often appeared flattened, displayed minimal migration, and had significantly more processes than cells on collagen (median of 7 with IQR of 4) (Fig. 2 *L* and *M*, *SI Appendix*, Fig. S4, and Movie S4).

CD49a and CD103 Are Unevenly Distributed on the Cell Surface and in Proximity to Respective Substrates in Tissue. We have shown that CD8 T cells can express CD49a and/or CD103 by flow cytometry and that these integrins provide distinct motility functions when examined in vitro. However, in both sets of experiments, cells were extracted from the tissues, which may not be representative of the entire population and does not indicate cellular location of the integrins (35). To identify the cellular localization of CD49a and CD103, tracheal tissue whole mounts from mice at days 14, 21, and 42 and 3 mo postinfection were stained and examined by microscopy. By day 14 postinfection, CD49a could be identified in proximity to collagen as measured by second-harmonic generation, directly underlying the epithelium (Fig. 3*A*). Within the epithelial layer, predominantly CD103-expressing cells were identified (Fig. 3*A*). At days 21 and 42 postinfection, it was clear that higher expression of these integrins on the cell surface was localized to specific foci, and it was more common to see expression of a single integrin type in a given region (Fig. 3 *B* and *C*). This suggested that some cells may be utilizing only one interaction or that a cell could be interacting with multiple substrates at distinct cellular regions simultaneously. By 3 mo postinfection, we observed a similar decrease in cells, as seen by flow cytometry, and identifying cells at this time point became more challenging. However, we could find small numbers of dual-expressing cells within the tissue as well as $CD103^+$ cells embedded within the epithelium (Fig. 3*D*). Of the cells identified at this time point within the epithelium, we could observe CD103 expression not only on the cell bodies but also on cellular processes in between epithelial cells (Fig. 3*D*). We were similarly able to identify $CD8^+$ cells in human trachea obtained from the Lung Development Molecular Atlas Program (LungMAP) consortium, the LungMAP Biorepository, and the LungMAP Data Coordinating Center. We observed CD103-expressing cells

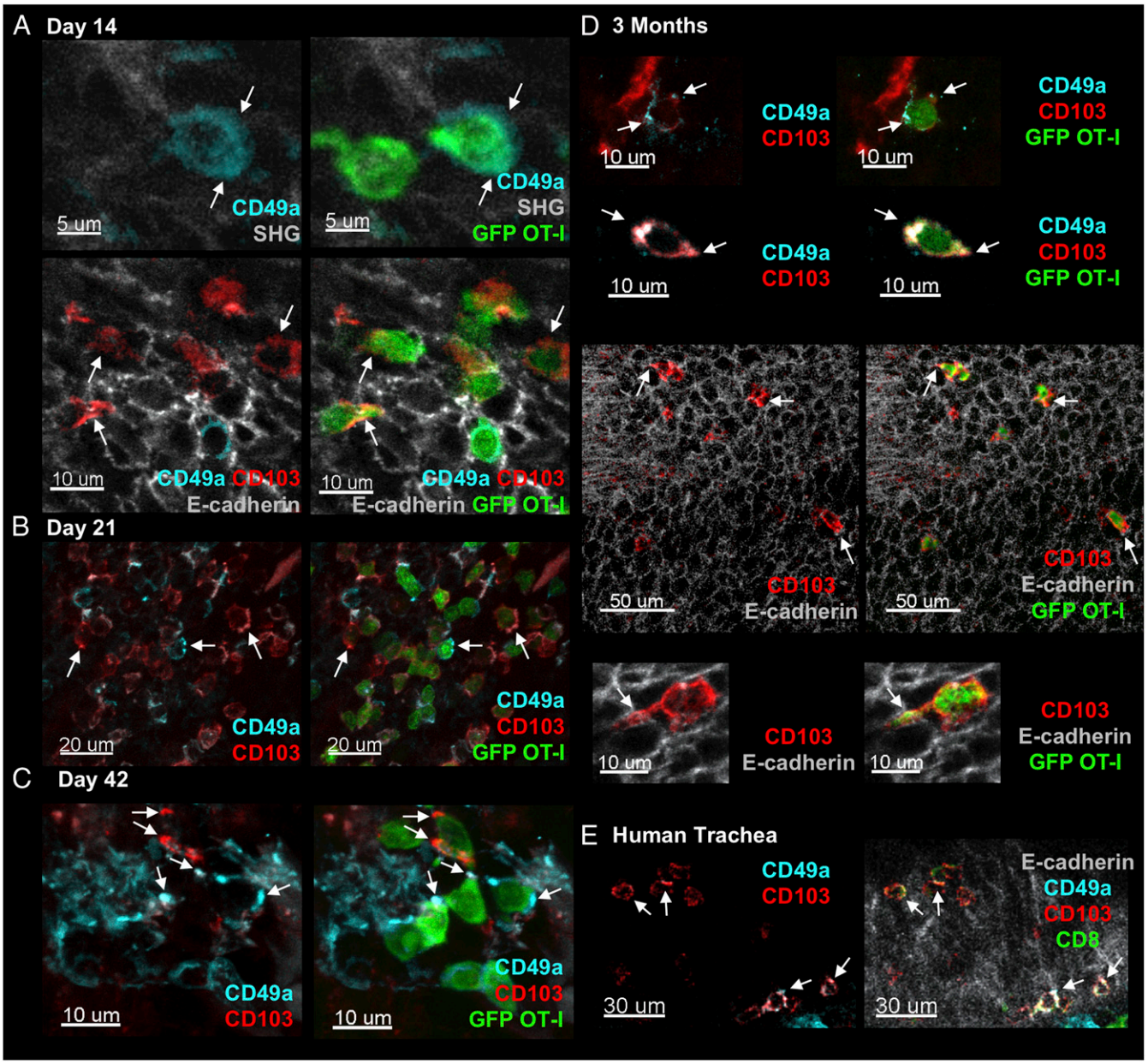

Fig. 3. CD49a and CD103 are expressed more highly in specific regions of cells and can be seen in proximity to integrin substrates. Tracheal whole mounts from mice that received GFP OT-I CD8 T cells prior to infection were stained for CD49a and CD103 where indicated. Tracheas were examined at days 14 (*A*), 21 (*B*), and 42 (*C*) and 3 mo (*D*) postinfection. Human tracheal whole mount was stained with anti-human CD8, CD49a, CD103, and E-cadherin (*E*). Arrows indicate regions of localized staining.

closer to the tip of the airway epithelial cells (upward-facing arrows) and dual-expressing $CD8^+$ cells closer to the basement membrane (Fig. 3*E*), suggesting that integrins on human CD8 T cells may employ similar interactions.

CD49a Promotes Motility and CD103 Limits Speed In Vivo. One main goal of this study was to evaluate the role(s) of these integrins in cell motility in vivo. To achieve this, we utilized an intravital tracheal imaging system, previously developed in the laboratory (36). Transgenic OT-I T cells from wild-type (WT) or integrin-deficient mice were transferred to wild-type hosts and imaged at 2 wk postinfection to examine CD8 T cell movement over time. In comparison to the simplistic 2D collagen system, wild-type cells observed in the trachea displayed fairly low speeds (median of 1.95 μm/min with an IQR of 1.82), without extensive displacement (median of 0.33 μm/min with an IQR of 0.41) (Fig. 4 *A–D* and Movie S5). This is likely due to the combination of signals the cells are receiving through multiple interactions and a consequence of being in a more confined environment. However, eliminating CD49a in GFP OT-I cells resulted in further limited motility, consistent with the concept that CD49a is facilitating locomotion on collagen IV (Fig. 4 *A–C* and *E* and Movie S6). Conversely, the absence of CD103 resulted in increased speeds compared with wild-type cells (Fig. 4 *A–C* and *F* and Movie S7). The number of cells at this time point, however, was reduced, so we employed a second approach to examine the contribution of CD103 in this system. Wild-type OT-I cells were transferred into naïve wild-type hosts, and starting on day 7 postinfection, mice were given a CD103-blocking antibody or isotype antibody every other day until imaging. To ensure the

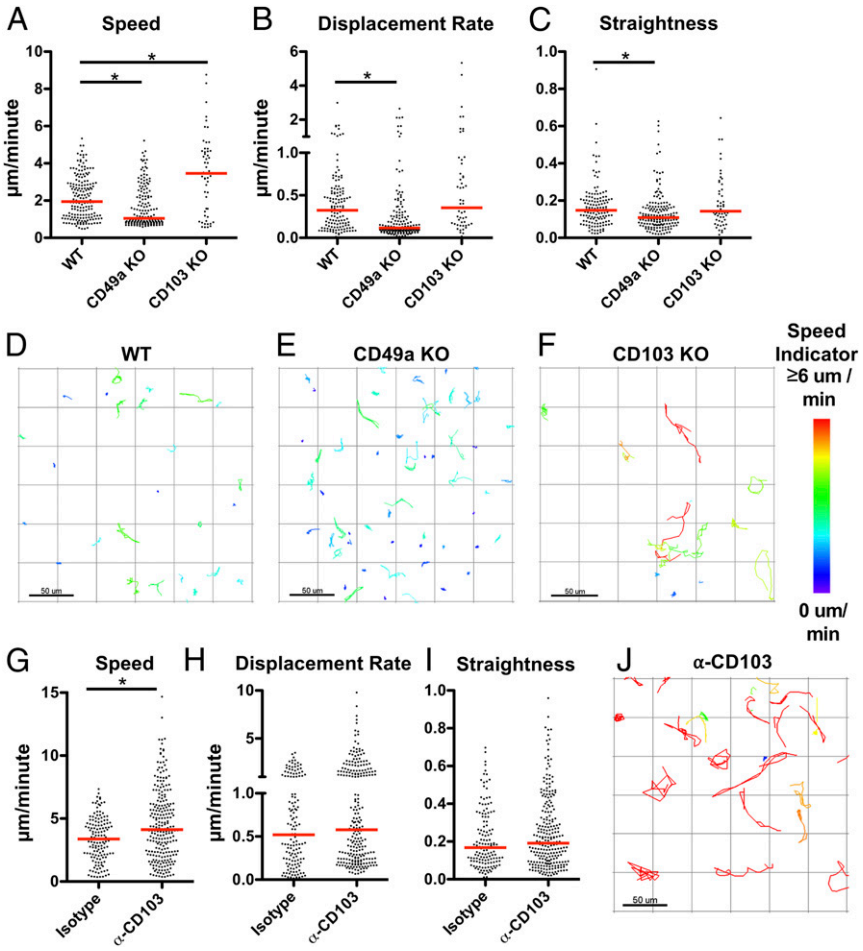

Fig. 4. CD49a facilitates motility, and CD103 limits speed. Integrin-sufficient and -deficient GFP OT-I CD8 T cells were adoptively transferred prior to infection with HKx31-OvaI influenza virus. Intravital imaging of the trachea was utilized to examine CD8 T cell motility in vivo on day 14 postinfection. Speed (*A*), displacement rate (*B*), and straightness (*C*) were enumerated. (*D–F*) Representative tracks are shown, with the color indicating the average track speed. Speed (*G*), displacement rate (*H*), and straightness (*I*) for CD103-blocking or isotype control treatment and representative tracks with CD103-blocking antibody (*J*). Data were combined from three to four mice for each condition. $*P < 0.05$.

antibody was reaching the cells, separate mice were examined for the presence of the antibody bound to virus-specific CD8 T cells, using an anti-rat IgG antibody. Cells in the trachea, lung, and airways of anti-CD103 treated mice were labeled with the anti-rat IgG, while isotype control mice showed no binding of the secondary antibody (*SI Appendix*, Fig. S5*A*). The absence of staining with the CD103 antibody prior to flow cytometric analysis suggested that not only was the in vivo antibody already bound but it was likely saturating. Blocking CD103 using this approach resulted in numbers of cells comparable to wild type on day 14 postinfection. However, the motility was markedly similar to that observed using the knockout cells. OT-I CD8 T cells displayed increased speeds in anti-CD103-treated mice compared with controls (Fig. 4 *G–J* and Movie S8). This effect was moderate, likely reflecting the fact that only about a third of CD8 T cells express CD103 and, therefore, two-thirds of the cells are unaffected by the antibody. The data support the conclusion that CD103 is not a mediator of motility, suggesting a role in localization and/or cell–tissue interactions.

CD49a and CD103 in T_{RM} Formation and Function. Both integrins have been implicated in the formation of T_{RM} in the tissue. To determine whether the absence of one or the other integrin affects the overall integrin phenotype early after viral clearance, cells were examined using flow cytometry after transfer of either WT or integrin-deficient cells on day 14 postinfection. In the absence of CD49a, no changes in the frequency or number of CD103 positive cells were observed (Fig. 5 *A* and *B*). Likewise, cells deficient in CD103 expressed similar frequencies of CD49a at this same time point (Fig. 5 *C* and *D*). The total number of CD103-deficient CD8 T cells expressing CD49a was slightly, but not significantly, decreased (Fig. 5*D*). However, this was not unexpected based on the in vivo data. Overall, our data suggest that the level of each integrin is regulated independently of the other. However, there could still be functional compensatory mechanisms.

Therefore, we next sought to determine whether CD49a and CD103 could equally contribute to host defense. Our laboratory previously showed a requirement for CD49a to protect a host from heterosubtypic influenza virus challenge at 3 mo post-infection (2). However, the contribution of CD103 in secondary protection has not been established. To examine this, WT and CD49a-deficient mice were infected with the H3N2 virus HKx31 to generate a pool of memory cells. Three days and 1 d prior to reinfection with H1N1 virus PR8, both genotypes of mice were given either CD103-blocking antibody or phosphate-buffered saline (PBS) control. Again, to ensure localization of the antibody, separate mice were examined for binding of a secondary

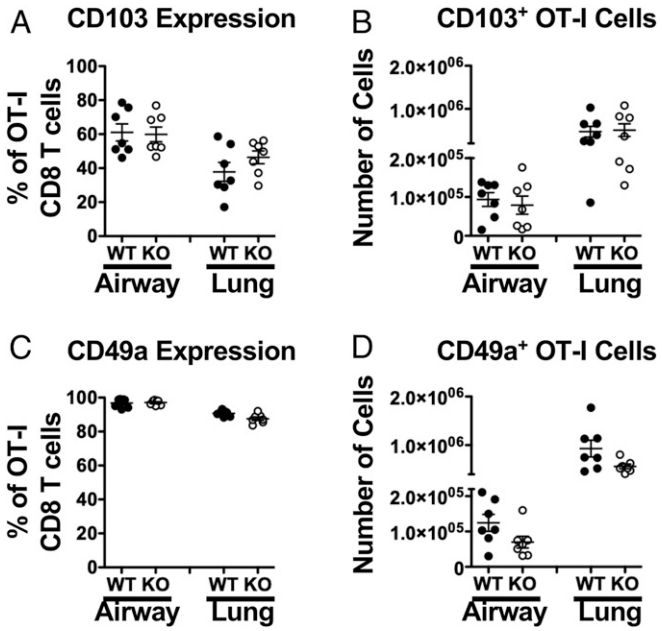

Fig. 5. CD49a and CD103 expression is not influenced by the absence of the other integrin. WT or integrin-deficient cells were transferred into WT mice prior to infection with HKx31-OvaI influenza virus. The airway (BAL) and lung were examined on day 14 postinfection for the presence of CD103 on WT and CD49a KO OT-I cells (*A* and *B*) or CD49a on WT and CD103 KO OT-I cells (*C* and *D*). Data are shown as a percentage of the OT-I T cell population or absolute number of cells. Data shown are two experiments combined.

antibody to show the presence of anti-CD103 (*SI Appendix*, Fig. S5*B*). CD49a-deficient mice, regardless of treatment, succumbed to the challenge by day 8, only 1 d later than nonimmune mice with no prior infection (Fig. 6 *A* and *B*). WT mice given CD103-blocking antibody were protected equally as well as mice given control treatment, and the majority of mice survived the challenge (Fig. 6 *A* and *B*). These data show a clear requirement for CD49a but further suggest that the CD103–E-cadherin interaction is not necessary at late time points for T_{RM}-mediated host protection.

Discussion

Integrins CD49a and CD103 appear on the surface of CD8 T cells in the airways, trachea, and lung tissue early after clearance of influenza virus, by day 14. While these integrins are viewed as markers of T_{RM} cells, they actually offer CD8 T cells the capacity to interact with collagen IV in the lamina densa underlying the epithelium, collagen I in the interstitium, and the epithelial cells directly through E-cadherin binding. The expression of CD49a and CD103 early after viral clearance suggests they are playing a critical role contributing to the development and maintenance of T_{RM}. Previous work has established that active TGF-β, which is present during disease resolution, is essential for expression of CD103 and CD49a (37). In the gut, this has been highlighted by eliminating TGF-β signaling to T cells, which results in continued recruitment of effector cells but no demonstrable population of tissue memory (37). Additionally, Nur77 signaling was recently linked to direct regulation of CD49a transcription in endothelial cells, potentially implicating a role for in situ TCR stimulation in modifying surface expression in this system (38, 39). Integrins can also be regulated through outside-in signaling, suggesting that direct interactions with collagen or E-cadherin on cells poised within or in proximity to the airway may enhance surface expression of CD49a or CD103, respectively (40).

Distinct subsets of CD8 T cells in the airway, lung tissue, and trachea can be identified through expression of CD49a and/or CD103. Early characterization of T_{RM} cells focused exclusively on CD103 and CD69 as identifiers of the population; however, our laboratory has shown that CD49a is critical for long-term maintenance of the population in the lungs, in part through survival signals received via interactions with collagen IV (2, 16). CD103 appears to regulate early recruitment and persistence but is less critical after resolution of infection for maintenance of the memory pool (21, 22). We sought to examine the outcomes of these integrins interacting with their ligands both in vitro and in vivo to reveal potential mechanisms regulating the T_{RM} population and ultimately host protection.

In vitro imaging of virus-specific CD8 T cells on collagen IV and E-cadherin suggested that only CD49a mediated locomotion in the context examined. CD8 T cells migrated readily on collagen IV in a CD49a-dependent manner. While previous reports examining other cell types such as fibroblasts and endothelial cells suggested that CD49a's function was primarily to adhere to collagen, the differences observed could be attributed to distinct mechanisms mediating adhesion between cell types (38, 41, 42). Inhibition or knockdown of CD49a in tumor cells resulted in decreased migration compared with their CD49a-sufficient counterparts (43, 44). Similarly, human CD8 T cells ex vivo were unable to migrate through a collagen IV–coated transwell when CD49a was blocked (18). More extensive examination of whether these CD8 T cells on collagen require active reengagement of ligand to survive long term is warranted, with the knowledge that the CD49a–collagen IV interactions are important for cell persistence. Additionally, it would be of interest to determine whether these outcomes are specific to collagen IV or if these phenomena can be more generally applied to other collagens, such as collagen I, which is distributed more broadly throughout the tissue. Alternatively, T cells on E-cadherin displayed attachment to the surface but exhibited limited migration. This could suggest a fundamentally different role in regulation of cell behavior, and this is consistent with both lymphoid and nonlymphoid cells examined in other organs such as the gut (33, 34). This interaction may mediate local retention of cells at the peripheral site and provide continued surveillance. While we observed an increase of cellular processes on the cells on E-cadherin, further investigation will be necessary to determine if this is due solely to the interaction between CD103 and E-cadherin or if this observed morphology is downstream of inside-out cytokine signals or requires the contribution of other adhesion molecules (20, 45). Salivary gland T_{RM} and some dendritic cells have been shown to express E-cadherin (46, 47), which could participate in binding through homotypic interactions.

Within the tissue, CD49a and CD103 are not uniformly distributed on the cell surface. In fact, we can find expression of

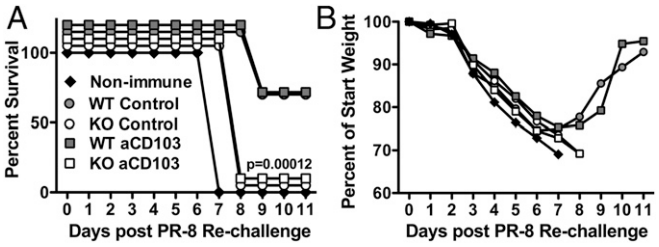

Fig. 6. CD49a, but not CD103, is necessary for heterosubtypic protection. WT or CD49a KO mice were infected with HKx31 influenza A virus. At 3 mo postinfection, mice were given either anti-CD103 or PBS as a control and challenged with a lethal dose of PR8 influenza A virus. Mice with no prior immunity (nonimmune) were included as controls. Mice were monitored daily for survival (*A*) and weight loss (*B*). $n = 3$–5 mice/group. Representative data are from one of two independent experiments.

each integrin in regions of the integrin ligand. CD103 coincided with E-cadherin expression within the epithelium, consistent with the capacity to interact with epithelial cells. CD49a could be identified in close proximity to collagen directly underlying epithelial cells, suggesting it may use this surface to explore other regions of the epithelium and receive prosurvival signals. To determine whether these integrins played similar roles in vivo to what was observed in vitro, we used a combination of genetically deficient T cells and blocking antibodies to examine the motility of virus-specific CD8 T cells in the trachea of 2 wk infected mice. Consistent with cell motility observed in the 2D setting, the absence of CD49a in vivo resulted in further arrest of the cells, indicating a role in cell locomotion. This observation conflicted with our initial interpretation that CD49a was important for retention by physically adhering the cells to the matrix. Instead, these studies reveal that CD49a is critical for cell motility, a feature that was not previously associated with retention. In contrast, knocking out or blocking CD103 resulted in increased speeds of the cells examined. While in vivo migration of T cells lacking CD49a has not been extensively examined, transplanted human skin in a mouse model of psoriasis showed that CD49a blockade limited the ability of T cells to position within the epidermal layer and sequestered these cells to the dermis, signifying an important role for CD49a in motility and/or positioning (18). Alternatively, imaging of CD103-deficient CD8 T cells in the skin during a mouse model of herpes simplex virus infection similarly displayed increased speeds, suggesting that CD103 restrains the cells' motility, possibly by affecting tissue localization or tissue interactions, which remain to be investigated (20).

For years, the CD8 T cell field has relied on using integrins CD103 and CD49a to identify the T_{RM} subset; however, our understanding of the functions of these receptors in regulating interactions with the tissue and T cell motility is incomplete and underappreciated. In this paper we examined the roles of CD103 and CD49a in the CD8 T cell subset present after clearance of viral infection. The absence or blocking of CD49a in this system showed an unexpectedly strong effect, indicating that other integrins such as CD51 which confer motility in CD4 T cells are not sufficient to compensate in this population (48). Alternatively, our data suggest that CD103's main function is not to mediate locomotion, possibly functioning mainly as an attachment to the epithelial surface and facilitating maintenance and surveillance. γδ T cells in the gut have been shown to "floss" the epithelium (49). We propose T_{RM} in the airways exhibits a similar behavior, and we cannot discount a role for CD103 in this context. Of note, while the effects observed were consistent both in vitro and in vivo, our analysis examined the complete pool of virus-specific CD8 T cells present in the tissue. Future experiments with more focused imaging and transcriptomics analyses will be needed to dissect how different integrin phenotypes regulate interactions within the tissues and their resulting cellular functions. It will also be of interest to determine how these integrins affect motility in response to secondary infection and further extend these findings to other organ systems and infections. Given the ubiquity of the ligands for CD49a and CD103 at mucosal and epithelial barriers, our data support the hypothesis that the mechanisms described here may extend beyond the pulmonary system and may be critical for secondary immune protection at boundary surfaces throughout the body.

Materials and Methods

Mice. All mice were housed in university-approved microisolator cages, within a pathogen-free facility. C57BL/6J mice (Jackson Laboratories) used for experiments were infected at 8 to 10 wk of age. OT-I GFP transgenic mice were maintained in house at the University of Rochester (36). This line of mice was crossed with VLA-1 knockout (KO) mice (2) or CD103 KO mice [B6.129S2(C)-Itgae^{tm1Cmp}/J] (Jackson Laboratories). This study was carried out in strict accordance with the recommendations in the *Guide for the Care and Use of Laboratory Animals* as defined by the NIH (50). Animal protocols were reviewed and approved by the Institutional Animal Care and Use Committee of the University of Rochester. All animals were housed in a centralized and Association for Assessment and Accreditation of Laboratory Animal Care accredited research animal facility that is fully staffed with trained husbandry, technical, and veterinary personnel.

Treatment and Cell Transfer. On day −1, 1×10^6 splenocytes from WT or integrin KO GFP OT-I cells were injected IV into naïve C57BL/6 hosts. WT and integrin KO mice were checked by flow cytometry to ensure that comparable numbers of CD8 T cells were being transferred. For CD103 blocking, mice were given 150 μg anti-CD103 antibody (clone M290) or isotype control antibody (clone 2A3) intraperitoneally in a 200 μL volume. Mice were given injections on days 7, 9, 11, and 13. For blocking prior to secondary challenge, mice were given 150 μg anti-CD103 or PBS on days −3 and −1 and 150 μg intranasally on day −2. For cellular preparations, 0.2 μg CD8β-FITC, CD45-PE, or CD45-Brilliant Violet 786 was given IV in 100 μL PBS 3 min prior to organ harvest.

Viruses and Infections. Mice were infected as previously described (36, 51). In brief, H3N2 A/Hong Kong/X31 (HKx31) influenza virus, HKx31-OVAI expressing the ovalbumin (OVA257-264 SIINFEKL) peptide in the neuraminidase viral protein, and H1N1 A/Puerto Rico/8 (PR8) were grown and titered in house in embryonated chicken eggs (27). Sedated mice were infected intranasally with 10^5 50% egg infectious dose (EID_{50}) of HKx31, 3×10^3 EID_{50} HKx31-OVAI, or 10^3 EID_{50} PR8 in 30 μL of PBS. Infected mice were monitored daily for weight loss and other signs of morbidity.

Cellular Preparations. Bronchoalveolar lavage (BAL), lung, and tracheal samples were prepared as previously described (51). Briefly, BAL was collected by flushing the lungs with 1× PBS, and samples were lysed with ACK lysis buffer (ammonium–chloride–potassium). Lungs and trachea were dissociated by the gentleMACS (Miltenyi Biotec) and were incubated in Collagenase II (Worthington) at 37 °C for 30 min, with gentle agitation. Cell suspensions were filtered and separated by a 75:40 Percoll (GE Healthcare) discontinuous gradient. Cell suspensions were counted on a hemocytometer, with trypan blue exclusion.

Flow Cytometry. Staining was achieved as previously described (51). Briefly, single-cell suspensions were stained in PBS with purified CD16/32 (clone 2.4G2); fixable live/dead indicator (Invitrogen); some combination of the antibodies TCRβ, CD8α, CD69, CD49a, CD103, and CD44 (Biolegend or BD Biosciences); and influenza tetramers (NP and PA) (NIH Tetramer Core Facility). Samples were run on an LSRII (BD Biosciences) and analyzed using FlowJo (Tree Star).

In Vitro Imaging. Cell migration chambers (Millicell EZ slide eight-well glass, Millipore, or Delta T dish, Biotech) were coated with 10 μg/cm^2 mouse collagen IV (Corning) in 0.05 M HCl for 1 h at room temperature or 2.5 μg/cm^2 mouse E-cadherin (R&D Systems) overnight at 4 °C in PBS. Prior to imaging, the plate was washed three times in PBS. For in vitro migration imaging, GFP OT-I cells were negatively enriched from lungs for CD8 T cells using the Miltenyi Biotec CD8 Isolation Kit (#130-104-075) and resuspended in L15 medium (Invitrogen) containing 2 mg/mL D-glucose. These cells were placed in the chamber at 37 °C and allowed to adhere for 20 min, and microscopy was conducted using a TE2000-U microscope (Nikon) coupled to a CoolSNAP HQ CCD camera with a 20× objective (CFI Plan Fluor ELWD DM; Nikon) and 0.45 numerical aperture. Cells were imaged for 20 min with images taken every 20 s. Blocking antibodies (1 μg) were added directly into the media, and cells were subsequently imaged for 20 min. All images were acquired in NIS Elements (Nikon). Migration analysis was performed in Imaris software (Bitplane). For TIRF microscopy, images were collected using a 60×/1.49 numerical aperture oil immersion TIRF objective (Nikon) placed on an inverted Ti-E microscope (Nikon) coupled to a Dragonfly TIRF module (Andor). Multifield time lapses were taken while samples were kept at 37 °C with 5% CO_2 with a stage top incubation system (Oko-Lab). For automated process detection in MATLAB, single Z plane TIRF images of cells over time were preprocessed for intensity thresholding prior to generating a binarized version (https://github.com/tophamlab20/projections/blob/master/projections.m). The Image Opening morphological filter was applied to identify the inside perimeter of the cell body. This created a new image that represented only the cell body, and subtraction of this image from the original generated potential cellular processes. Object detection and local thresholding were used to distinguish cellular processes from noise. Finally, each cellular process was labeled and counted, and the number of processes for each cell at a

given time point was returned. Cellular processes were also quantified manually, and the data comparison is provided in *SI Appendix*, Fig. S4*B*.

Tracheal Whole-Mount Imaging. Excised mouse trachea was incubated in PBS serum, anti-CD16/32, and indicated antibodies for 4 h at room temperature. The following antibodies were used in different combinations at the indicated dilutions: CD103–Alexa Fluor 594 (Biolegend), 1:50; CD49a-Alexa Fluor 647 (BD Biosciences), 1:25; and E-cadherin–APC (Biolegend) 1:50. Images were acquired on an Olympus FV1000 (Center for Advanced Light Microscopy and Nanoscopy Shared Resource Laboratory) using an Olympus Plan Apo 60×/1.43 NA objective. Fresh, transplant donor–quality human tracheal tissue was obtained from the Human Tissue Core of LungMAP at the University of Rochester. The University of Rochester Institutional Review Board approved and oversees this study (approval no. RSRB00047606). Human trachea was stained for 72 h in PBS serum and the following Biolegend antibodies: hCD103–Alexa Fluor 594, 1:40; hCD8–Alexa Fluor 488, 1:40; hCD49a–Alexa Fluor 647, 1:40; and E-cadherin–APC, 1:40. Human tissue was washed in PBS and fixed in 4% paraformaldehyde for 2 h prior to mounting. Mouse tissue was washed in PBS and mounted unfixed. All whole-mount tissue sections were mounted using Fluoromount-G (SouthernBiotech).

Intravital Multiphoton Imaging. Intravital tracheal imaging was performed as described in Lambert Emo et al. (36). Briefly, mice were anesthetized with 65 mg/kg pentobarbital. Hair was removed from one hind leg, exposing skin for MouseOX Plus sensor (Starr Life Sciences) monitoring. The hair was removed from the thoracic area with scissors, and the mouse was placed on a heated stage. Once the surgical plane of anesthesia was determined by both lack of pedal and palpebral reflex, the coat was opened between the chin and the top of the rib cage. The submandibular salivary glands were separated to reveal the muscles covering the trachea, and these muscles were separated to expose the trachea. A small flexible plastic support was placed under the trachea to separate it from the surrounding muscle, tissue, and coat. A small incision was made between cartilage rings below the larynx. An 18-gauge steel cannula was inserted into the opening in the trachea until just below the sternum. Mice were ventilated through the cannula using the Harvard Inspira ASV ventilator with 100% oxygen and 0.5% isoflurane according to weight. The MouseOX Plus thigh sensor was attached to the exposed thigh, and the mouse was monitored throughout the imaging session. Oxygenation levels were maintained at >95%, and heart rate was maintained between 250 and 600 beats per minute. The rectal body temperature was monitored and maintained using a small-animal feedback regulated heating pad. After the animal was stable and reverification of the lack of both pedal and palpebral reflex, pancuronium bromide (0.4 mg/kg) was administered intramuscularly. Agarose (0.05%) was added to the exposed trachea, and plastic wrap was used to create a water basin for the objective.

All images were collected by an Olympus FVMPE-RS system (Olympus) using an Olympus 25× water objective (XLPLN25XWMP2, 1.05 NA). The system was equipped with two two-photon lasers: Spectra-Physics InSightX3 (680 to 1,300 nm, Spectra-Physics) and Spectra-Physics MaiTai DeepSee Ti:sapphire laser (690 to 1,040 nm). There were four photon multiplier tubes (PMTs) and two filter cubes (blue/green cube: 420 to 460 nm/495 to 540 nm, red/fRed cube: 575 to 630 nm/645 to 685 nm) for multicolor imaging. A galvonometer scanner was used for scanning, and all images were acquired at ∼1 frame/s. PMT gains for all imaging were used between 550 and 700 a.u. in the Olympus Fluoview software. All images were registered within MATLAB (MathWorks) using the registration code provided by the Center for Integrated Research Computing (https://github.com/TophamLab/Registration) and were analyzed and visualized using Imaris (Bitplane) software.

Statistics. The majority of statistics were performed using Prism analysis software (GraphPad). Flow cytometry data groups were compared using a Student's *t* test and are shown as mean and SD. For imaging data which cannot be assumed to be normally distributed, the Kruskal–Wallis test was performed, followed by Dunn's comparisons with the control group. Mean fluorescence intensity data were compared with a paired *t* test. Significance was considered a P value < 0.05. Imaging data values are presented as median and IQR. For survival data a nonparametric Kaplan–Meier method was applied. For the analysis of the cell process data, nonparametric mixed-effect models by a cubic smoothing spline were used to model cell processes on the surface. Smoothing parameters were determined by the generalized cross-validation criterion. As *SI Appendix*, Fig. S4 indicates, the number of processes on cells on E-cadherin were higher than the number of processes of cells on collagen IV between time 0 and 40 (not including 0 and 40) since 95% CIs for the former top those for the latter and there is no overlap in the CIs.

Data Availability. The data supporting this publication are available at ImmPort under study accession SDY1631 (https://www.immport.org) (52).

ACKNOWLEDGMENTS. The authors would like to thank the Flow Cytometry Core, the Multiphoton and Analytical Imaging Center, and the Center for Advanced Light Microscopy and Nanoscopy at the University of Rochester. The authors also thank the Center for Integrated Research Computing at the University of Rochester for providing computational resources and technical support. The human data shown in this paper were made possible through the LungMAP Consortium (Grant U01HL122642), the LungMAP Biorepository (Grant 1U01HL122700), and the LungMAP Data Coordinating Center (Grant 1U01HL122638), which are funded by the National Heart, Lung, and Blood Institute. The authors would also like to thank the Kim laboratory at the University of Rochester for generously allowing us to utilize their microscope for in vitro imaging studies. This work was supported by NIH/National Institute of Allergy and Infectious Diseases Grant P01 AI102851. Funding was provided by NIH Research Grant P01 AI102851.

1. D. Masopust, J. Jiang, H. Shen, L. Lefrançois, Direct analysis of the dynamics of the intestinal mucosa CD8 T cell response to systemic virus infection. *J. Immunol.* **166**, 2348–2356 (2001).
2. S. J. Ray *et al*., The collagen binding alpha1beta1 integrin VLA-1 regulates CD8 T cell-mediated immune protection against heterologous influenza infection. *Immunity* **20**, 167–179 (2004).
3. K. H. Ely, T. Cookenham, A. D. Roberts, D. L. Woodland, Memory T cell populations in the lung airways are maintained by continual recruitment. *J. Immunol.* **176**, 537–543 (2006).
4. T. Wu *et al*., Lung-resident memory CD8 T cells (TRM) are indispensable for optimal cross-protection against pulmonary virus infection. *J. Leukoc. Biol.* **95**, 215–224 (2014).
5. K. Houser, K. Subbarao, Influenza vaccines: Challenges and solutions. *Cell Host Microbe* **17**, 295–300 (2015).
6. M. L. DeDiego, K. Chiem, D. J. Topham, Directed selection of amino acid changes in the influenza hemagglutinin and neuraminidase affecting protein antigenicity. *Vaccine* **36**, 6383–6392 (2018).
7. A. Cushing *et al*., Emergence of hemagglutinin mutations during the course of influenza infection. *Sci. Rep.* **5**, 16178 (2015).
8. H. Shin, A. Iwasaki, A vaccine strategy that protects against genital herpes by establishing local memory T cells. *Nature* **491**, 463–467 (2012).
9. K. D. Klonowski *et al*., Dynamics of blood-borne CD8 memory T cell migration in vivo. *Immunity* **20**, 551–562 (2004).
10. S. Takamura *et al*., Specific niches for lung-resident memory CD8+ T cells at the site of tissue regeneration enable CD69-independent maintenance. *J. Exp. Med.* **213**, 3057–3073 (2016).
11. T. Gebhardt, L. K. Mackay, Local immunity by tissue-resident CD8(+) memory T cells. *Front. Immunol.* **3**, 340 (2012).
12. D. J. Topham, E. C. Reilly, Tissue-resident memory CD8$^+$ T cells: From phenotype to function. *Front. Immunol.* **9**, 515 (2018).
13. Y. T. Lee *et al*., Environmental and antigen receptor-derived signals support sustained surveillance of the lungs by pathogen-specific cytotoxic T lymphocytes. *J. Virol.* **85**, 4085–4094 (2011).
14. L. K. Mackay *et al*., Cutting edge: CD69 interference with sphingosine-1-phosphate receptor function regulates peripheral T cell retention. *J. Immunol.* **194**, 2059–2063 (2015).
15. D. A. Walsh *et al*., The functional requirement for CD69 in establishment of resident memory CD8$^+$ T cells varies with tissue location. *J. Immunol.* **203**, 946–955 (2019).
16. M. V. Richter, D. J. Topham, The alpha1beta1 integrin and TNF receptor II protect airway CD8+ effector T cells from apoptosis during influenza infection. *J. Immunol.* **179**, 5054–5063 (2007).
17. E. J. Meharra *et al*., Reduced gut intraepithelial lymphocytes in VLA1 null mice. *Cell. Immunol.* **201**, 1–5 (2000).
18. C. Conrad *et al*., Alpha1beta1 integrin is crucial for accumulation of epidermal T cells and the development of psoriasis. *Nat. Med.* **13**, 836–842 (2007).
19. L. K. Mackay *et al*., The developmental pathway for CD103(+)CD8+ tissue-resident memory T cells of skin. *Nat. Immunol.* **14**, 1294–1301 (2013).
20. A. Zaid *et al*., Chemokine receptor-dependent control of skin tissue-resident memory T cell formation. *J. Immunol.* **199**, 2451–2459 (2017).
21. B. S. Sheridan *et al*., Oral infection drives a distinct population of intestinal resident memory CD8(+) T cells with enhanced protective function. *Immunity* **40**, 747–757 (2014).
22. J. T. Thom, T. C. Weber, S. M. Walton, N. Torti, A. Oxenius, The salivary gland acts as a sink for tissue-resident memory CD8(+) T cells, facilitating protection from local cytomegalovirus Infection. *Cell Rep.* **13**, 1125–1136 (2015).
23. M. Barczyk, S. Carracedo, D. Gullberg, Integrins. *Cell Tissue Res.* **339**, 269–280 (2010).
24. I. D. Campbell, M. J. Humphries, Integrin structure, activation, and interactions. *Cold Spring Harb. Perspect. Biol.* **3**, a004994 (2011).
25. L. R. Shiow *et al*., CD69 acts downstream of interferon-alpha/beta to inhibit S1P1 and lymphocyte egress from lymphoid organs. *Nature* **440**, 540–544 (2006).

26. A. J. Bankovich, L. R. Shiow, J. G. Cyster, CD69 suppresses sphingosine 1-phosophate receptor-1 (S1P1) function through interaction with membrane helix 4. *J. Biol. Chem.* **285**, 22328–22337 (2010).
27. M. R. Jenkins, R. Webby, P. C. Doherty, S. J. Turner, Addition of a prominent epitope affects influenza A virus-specific CD8+ T cell immunodominance hierarchies when antigen is limiting. *J. Immunol.* **177**, 2917–2925 (2006).
28. K. G. Anderson *et al*., Cutting edge: Intravascular staining redefines lung CD8 T cell responses. *J. Immunol.* **189**, 2702–2706 (2012).
29. K. G. Anderson *et al*., Intravascular staining for discrimination of vascular and tissue leukocytes. *Nat. Protoc.* **9**, 209–222 (2014).
30. P. Vandenberg *et al*., Characterization of a type IV collagen major cell binding site with affinity to the alpha 1 beta 1 and the alpha 2 beta 1 integrins. *J. Cell Biol.* **113**, 1475–1483 (1991).
31. D. Gullberg *et al*., Analysis of alpha 1 beta 1, alpha 2 beta 1 and alpha 3 beta 1 integrins in cell–collagen interactions: Identification of conformation dependent alpha 1 beta 1 binding sites in collagen type I. *EMBO J.* **11**, 3865–3873 (1992).
32. A. Kern, J. Eble, R. Golbik, K. Kühn, Interaction of type IV collagen with the isolated integrins alpha 1 beta 1 and alpha 2 beta 1. *Eur. J. Biochem.* **215**, 151–159 (1993).
33. K. L. Cepek, C. M. Parker, J. L. Madara, M. B. Brenner, Integrin alpha E beta 7 mediates adhesion of T lymphocytes to epithelial cells. *J. Immunol.* **150**, 3459–3470 (1993).
34. K. L. Cepek *et al*., Adhesion between epithelial cells and T lymphocytes mediated by E-cadherin and the alpha E beta 7 integrin. *Nature* **372**, 190–193 (1994).
35. E. M. Steinert *et al*., Quantifying memory CD8 T cells reveals regionalization of immunosurveillance. *Cell* **161**, 737–749 (2015).
36. K. Lambert Emo *et al*., Live imaging of influenza infection of the trachea reveals dynamic regulation of CD8+ T cell motility by antigen. *PLoS Pathog.* **12**, e1005881 (2016).
37. N. Zhang, M. J. Bevan, Transforming growth factor-β signaling controls the formation and maintenance of gut-resident memory T cells by regulating migration and retention. *Immunity* **39**, 687–696 (2013).
38. T. Ye *et al*., Orphan nuclear receptor TR3/Nur77 differentially regulates the expression of integrins in angiogenesis. *Microvasc. Res.* **122**, 22–33 (2019).
39. N. R. Cunningham *et al*., Immature CD4+CD8+ thymocytes and mature T cells regulate Nur77 distinctly in response to TCR stimulation. *J. Immunol.* **177**, 6660–6666 (2006).
40. B. Shen, M. K. Delaney, X. Du, Inside-out, outside-in, and inside-outside-in: G protein signaling in integrin-mediated cell adhesion, spreading, and retraction. *Curr. Opin. Cell Biol.* **24**, 600–606 (2012).
41. M. Walraven, S. J. van Vliet, R. H. Beelen, M. van Egmond, M. M. Ulrich, Blocking α1-integrin reverts the adhesive phenotype of adult fibroblasts towards a foetal-like migratory phenotype. *Exp. Dermatol.* **25**, 480–482 (2016).
42. J. T. Parsons, Focal adhesion kinase: The first ten years. *J. Cell Sci.* **116**, 1409–1416 (2003).
43. L. M. Moir, J. L. Black, V. P. Krymskaya, TSC2 modulates cell adhesion and migration via integrin-α1β1. *Am. J. Physiol. Lung Cell. Mol. Physiol.* **303**, L703–L710 (2012).
44. S. Boudjadi *et al*., Involvement of the integrin α1β1 in the progression of colorectal cancer. *Cancers* **9**, E96 (2017).
45. A. Ericsson, M. Svensson, A. Arya, W. W. Agace, CCL25/CCR9 promotes the induction and function of CD103 on intestinal intraepithelial lymphocytes. *Eur. J. Immunol.* **34**, 2720–2729 (2004).
46. K. R. Siddiqui, S. Laffont, F. Powrie, E-cadherin marks a subset of inflammatory dendritic cells that promote T cell-mediated colitis. *Immunity* **32**, 557–567 (2010).
47. M. Hofmann, H. Pircher, E-cadherin promotes accumulation of a unique memory CD8 T-cell population in murine salivary glands. *Proc. Natl. Acad. Sci. U.S.A.* **108**, 16741–16746 (2011).
48. A. Gaylo, M. G. Overstreet, D. J. Fowell, Imaging CD4 T cell interstitial migration in the inflamed dermis. *J. Vis. Exp.*, e53585 (2016).
49. D. P. Hoytema van Konijnenburg *et al*., Intestinal epithelial and intraepithelial T cell crosstalk mediates a dynamic response to infection. *Cell* **171**, 783–794.e13 (2017).
50. National Research Council, *Guide for the Care and Use of Laboratory Animals*, (National Academies Press, Washington, DC, ed. 8, 2011).
51. E. C. Reilly, K. Lambert-Emo, D. J. Topham, The effects of acute neutrophil depletion on resolution of acute influenza infection, establishment of tissue resident memory (TRM), and heterosubtypic immunity. *PLoS One* **11**, e0164247 (2016).
52. D. J. Topham, Data from TRM integrins CD103 and CD49a differentially support adherence and motility after resolution of influenza virus infection. ImmPort. https://www.immport.org/shared/study/SDY1631. Deposited 5 May 2020.